AIAA JOURNAL
Vol. 31, No. 8, August 1993

Downstream Evolution of Proper Orthogonal Decomposition Eigenfunctions in a Lobed Mixer

L. Ukeiley,* M. Glauser,† and D. Wick*
Clarkson University, Potsdam, New York 13699

A two-dimensional (one space and time) scalar adaptation of the proper orthogonal decomposition was applied to streamwise velocity data obtained in a lobed mixer flowfield, using a rake of 15 single-component hot wires. Through the application of the proper orthogonal decomposition, the amount of streamwise turbulent kinetic energy contained in the various proper orthogonal modes was examined for two different downstream locations ($z/h = 2.6$ and 3.9). The large eddy or dominant mode was shown to have a measurable decrease in the relative streamwise component of the kinetic energy between these two downstream locations. This indicates that the large eddy, as defined by the proper orthogonal decomposition, breaks down, and the flow becomes more homogeneous. A pseudoflow visualization technique was then employed to help visualize this process.

Nomenclature

a_n = random coefficient
h = lobe width
l = lobe height
q = counter for eigenmodes
R_{11} = streamwise velocity cross-correlation tensor
u = velocity vector field
u_1 = instantaneous streamwise velocity
$\hat{u}_1$ = Fourier transform of streamwise velocity
u' = streamwise rms velocity
x = horizontal direction across lobes
y = vertical distance across lobes
$\bar{y}$ = vertical location of rake for data collection
z = streamwise direction
$\bar{z}$ = streamwise location of rake for data collection
$\lambda(f)$ = eigenspectra of streamwise turbulent kinetic energy
Φ_{ij} = cross-spectral tensor
ψ_i = eigenvector in transform domain

Introduction

A LOBED mixer is a device that induces rapid mixing through the enhancement of the streamwise vorticity. Physically, it is best described as a flat plate with a corrugated trailing edge (see Ukeiley et al.[1] and Werle et al.[2]). These mixers are currently being used to rapidly mix hot turbine exhaust gases with cool bypass flows in turbofan engines, greatly reducing the noise. Paterson[3] collected the first detailed velocity measurements in a practical lobed mixer flowfield. The study showed strong secondary flows along with streamwise vorticity with a spatial extent approximately equivalent to the lobe height. A later study (Werle et al.[2]) showed the flowfield downstream of the lobed mixer could be broken up into three distinct flow development regions. In the first region, the streamwise vortex tubes began to develop, became fully developed in the second, and dissipated in the third. Eckerle et al.[4] conducted a study, in the same facility used in this work, using a laser doppler anemometer (LDA). They documented that the three regions reported by Werle et al.[2] could be shifted by changing the velocity ratio across the lobes. For a 2:1 velocity ratio they found that the vortices in the shear layer right below the high-speed side decayed at a significantly greater rate than those generated from the shear layer right below the low-speed side. It was also deduced from their results that the seeds of the large-scale mean secondary flows originate from the boundary layer of the lobed mixer. Koutmos and McGuirk[5] studied mean velocity and turbulent kinetic energy profiles at many locations downstream of an axisymmetric lobed mixer with the use of an LDA. They found the gradients in the mean streamwise velocity and kinetic energy profiles were mixed out by around three lobe heights; however, it took slightly over five lobe heights to mix out the gradients in the profiles of the mean secondary flows. Ukeiley et al.[6] conducted a study in the same facility being examined here with the use of a pseudoflow visualization technique (Delville et al.[7]). They examined the flowfield at four downstream positions and five horizontal positions across the center two lobes (the testing area in Fig. 1). Their results indicated the two streams were effectively mixed out by $z/h = 3.9$. Kock am Brink and Foss[8] conducted a study comparing the shear layers generated by both a rippled trailing-edge plate (a lobed mixer) and a planar trailing plate with the use of a multisensor hot-wire technique. Along with an extensive study of the boundary layer, they showed that the rippled

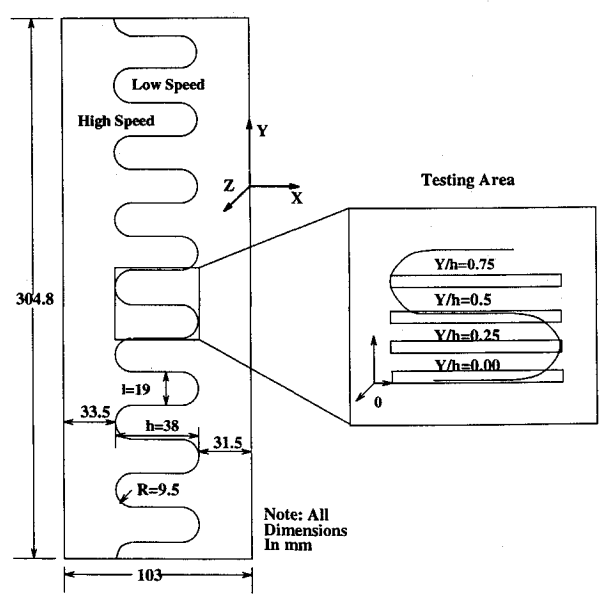

Fig. 1 Front view of lobed mixer.

Received March 13, 1992; revision received Nov. 15, 1992; accepted for publication Nov. 28, 1992.

*Graduate Research Assistant, Department of Mechanical and Aeronautical Engineering. Student Member AIAA.
†Associate Professor, Department of Mechanical and Aeronautical Engineering. Member AIAA.

plate develops a wider range of vortical fluid in a shorter distance than the planar plate. They also concluded that the turbulent kinetic energy becomes more evenly distributed at the expense of the secondary mean flow. In a study by Lasheras and Choi[9] the effects of a periodically perturbed plate on a shear layer with a velocity ratio of 2:1 were examined (similar to the study here but at much lower velocities and with smaller lobe penetration). This was done in an attempt to study the instabilities that form the three-dimensional structure. It was found that counter-rotating streamwise vortical structures were embedded in the braids of connecting consecutive von Kármán vortices.

Lumley[10,11] suggested using the proper orthogonal decomposition (POD) technique to objectively identify large-scale structures or "large eddies" in a turbulent flow. The POD decomposes the flowfield in the inhomogeneous directions into an orthogonal set of modes. The selection of these modes is unbiased and ordered based on kinetic energy, with the first mode representing the structure with the most energy, i.e., the *large-scale* structure. Several authors have used this technique in various turbulent flows and for the study of systems exhibiting nonlinear behavior.[1,12-17]

In the study presented here, multipoint hot-wire measurements were used to obtain the cross-spectral tensor needed to apply a two-dimensional scalar version of the POD in the lobed mixer flow. Measurements of the streamwise velocity were taken, with a 2:1 velocity ratio, at two downstream locations ($z/h = 2.6$ and 3.9) and four cross-lobe positions ($y/h = 0.0$, 0.25, 0.5, and 0.75). The two downstream locations were selected because it has been previously shown, using pseudoflow visualization, that the structures evolve and break down in this region (Ukeiley et al.[6]). Through the use of the POD, the energy content of the large-scale structures is studied at various locations in the flow. The degree of the inhomogeneity in the streamwise direction is then inferred from the streamwise evolution of the spanwise spatial structure of the POD eigenfunctions.

Proper Orthogonal Decomposition

In 1967 Lumley[10] proposed the POD as an unbiased procedure for identifying large-scale structures in turbulent flows. It is based on decomposing the inhomogeneous directions in the flow into orthogonal modes using the Karhunen-Loeve expansion.[18] In the lobed mixer all three spatial directions are inhomogeneous to varying degrees, but the time direction is statistically stationary. The POD reduces to the harmonic decomposition in directions that are either homogeneous or stationary; hence Fourier modes were implemented in the time direction. With these conditions the following eigenvalue problem is appropriate:

$$\int \Phi_{ij}(x, x', y, y', z, z', f)\psi_j^{(n)}(x', y', z', f)\,dx'\,dy'\,dz' = \lambda^{(n)}(f)\psi_i^{(n)}(x, y, z, f) \tag{1}$$

For a more detailed explanation of the application in the lobed mixer, see Ukeiley et al.[1]

As an initial step in analyzing this flow, only a two-dimensional (one space and time) scalar version of the POD is applied. The application involves obtaining the cross-spectral tensor in the cross-lobe direction (x) and then solving the following integral eigenvalue problem:

$$\int \Phi_{11}(x, x', \bar{y}, \bar{z}, f)\psi_1^{(n)}(x', \bar{y}, \bar{z}, f)\,dx' = \lambda^{(n)}(f)\psi_1^{(n)}(x, \bar{y}, \bar{z}, f) \tag{2}$$

In Eq. (2) only the spanwise direction x is decomposed through the use of POD. The cross-lobe and streamwise directions are also statistically inhomogeneous in this flow but are not decomposed directly in this initial study. It should be noted that the streamwise and cross-lobe directions are not completely neglected since the spanwise eigenvalue problem is solved (independently) at four different cross-lobe positions for two downstream locations. Hence this gives some insight into the inhomogeneity in the streamwise and vertical directions. For the remaining part of this discussion $\bar{y}$ and $\bar{z}$ will be dropped because they are not variables but only denote fixed locations in space.

The eigenmodes obtained from Eq. (2) are orthonormal and can be used to reconstruct the original velocity field (its time Fourier transform) in the following manner:

$$\hat{u}_1(x, f) = \sum_{n=1}^{\infty} a_n(f)\psi_1^{(n)}(x, f) \tag{3}$$

where the random coefficients $a_n(f)$, in the previous equation, are calculated by

$$a_n(f) = \int \hat{u}_1(x, f)\psi_1^{(n)*}(x, f)\,dx \tag{4}$$

The original velocity field (and/or the contributions from the various POD modes) can then be obtained by inverse Fourier transforming $\hat{u}_1(x, f)$ to arrive at $\hat{u}_1(x, t)$. It is important to note that, to reconstruct the instantaneous velocity field, the velocities at every location must be sampled simultaneously, i.e., a rake of hot wires is necessary so that the various a' can be found from application of Eq. (4).

The numerical approximation, detailed by Glauser et al.,[19] simply consists of replacing the integral in Eq. (2) by an appropriate quadrature rule (in this study a trapezoidal rule). Then $\Phi_{11}(x, x', f)$ is obtained from experimental measurements at the different spatial locations examined and used in Eq. (2) to obtain the eigenvalues and eigenfunctions. These eigenfunctions and eigenvalues are then used to reconstruct the original random velocity field as well as the rms streamwise velocity and comparisons made between the various spatial locations.

Experiment

The facility used in this experiment, described in detail in Ukeiley et al.,[1] is split down the center by a steel plate with separately controlled blowers on either side to allow for various velocity ratios across the lobe. A front view of the test section with the contours of the lobed mixer superimposed on it is shown in Fig. 1. The lobed mixer was molded from fiberglass and consists of 15 full lobes with a 37.5% penetration ratio. The lobes have a width h of 0.038 m and a height l of 0.019 m. The flow conditions at the inlet to the test section were documented by Eckerle et al.[4] They found that the boundary layers on the plate were turbulent with an approximate 1% turbulence intensity in the core flow. A rake of hot wires was placed in the downstream flowfield of the lobed mixer at several y/h locations (see Fig. 1) for both $z/h = 2.6$ and 3.9. Detailed results are presented for $y/h = 0.75$. The coordinate system is shown in this figure where x, y, and z denote the cross-stream, cross-lobe, and streamwise coordinates, respectively, and zero is located at the left-hand corner of the testing area. The velocity on the low-speed side was 15 m/s, and that on the high-speed side was 30 m/s, resulting in a velocity ratio across the lobes of 2:1. These velocities resulted in a mean across the lobes of 22.5 m/s that was used to normalize the graphs presented in this work.

The hot-wire rake (Ukeiley et al.[20]) consisted of 15 probes evenly spaced across a full lobe width, with each individual wire connected to an A.A. Labs CTA anemometer. The sensing wires were 1 mm in length and were constructed from 5-μ tungsten wire, resulting in a length-to-diameter ratio of 200. The hot wires were calibrated using a polynomial scheme as detailed by George et al.[21] A personal computer-based data acquisition system, consisting of a Zenith 248 computer, a MetraByte DAS-20 simultaneous sample, and hold A/D converter (16 channel, 12 bit), was employed to collect the data. All channels were sampled at a rate of 3 kHz and low-pass filtered at 1.4 kHz. To ensure an adequate statistical sample for the cross-spectral tensor and the various single point moments, 100 blocks of 256 samples/block were taken.

Results

The following section will be broken into three subsections that deal with various unique applications of the POD in this flowfield. In the first section, entitled "Convergence of the POD," the convergence of the streamwise turbulent kinetic energy is examined at all locations. In the second section, entitled "Eigenfunctions," the spatial behavior of the eigenfunctions and the convergence of the rms streamwise velocities are presented for $z/h = 2.6$ and 3.9 at $y/h = 0.75$. In the final section, entitled "Instantaneous Velocity," the instantaneous velocity traces and various POD reconstructions of them are examined through the use of a pseudoflow visualization technique for $z/h = 2.6$ and 3.9 at $y/h = 0.75$.

Convergence of the POD

The relative streamwise kinetic energy is given, for the summation of up to the qth POD mode, as

$$E^q = \frac{\sum_{n=1}^{q} \int \lambda^{(n)}(f)\, df}{\sum_{n=1}^{N} \int \lambda^{(n)}(f)\, df} \tag{5}$$

As q goes to N, where N is the total number of eigenvalues and eigenfunctions, the value of E^q will approach 1. Figure 2 shows values of E^q plotted vs q for both downstream locations at $y/h = 0.75$ (similar behavior was observed for the other y/h positions). From this curve it can be inferred that the larger scales, represented by the first few modes, contain the majority of the energy at $z/h = 2.6$. In contrast to this, the curve representing $z/h = 3.9$ shows a not as significant dominant mode with the remaining energy being distributed more evenly over the POD modes (scales). Table 1 presents the percentage of energy contained in the eigenspectral modes for all positions where the rake was placed. The *relative* percentage of energy contained in the dominant mode is noticeably larger at $z/h = 2.6$ than at $z/h = 3.9$. This suggests that the energy is distributed over a wider range of scales by the second station downstream of the lobed mixer, which is consistent with the single-point measurements of Koutmos and McGuirk[5] and Eckerle et al.[4] These results would also indicate that the large-scale features (first POD mode) have been somewhat dissipated between $z/h = 2.6$ and 3.9. It is also interesting to note that at $z/h = 2.6$ the first POD mode associated with the secondary shear layer below the high-speed side at $y/h = 0.0$ contains significantly less relative energy (27%) than the one associated with the secondary shear layer below the low-speed side at $y/h = 0.5$ (41%). This is consistent with the results of Eckerle et al.[4] where two distinctly different decay rates for the counter-rotating streamwise vortices were found. It also demonstrates the statistical inhomogeneity in the vertical direction. In contrast the large-scale structures associated with the lobe troughs ($y/h = 0.25$ and 0.75) appear to decay at the same rate (32 vs 34%) by $z/h = 3.9$.

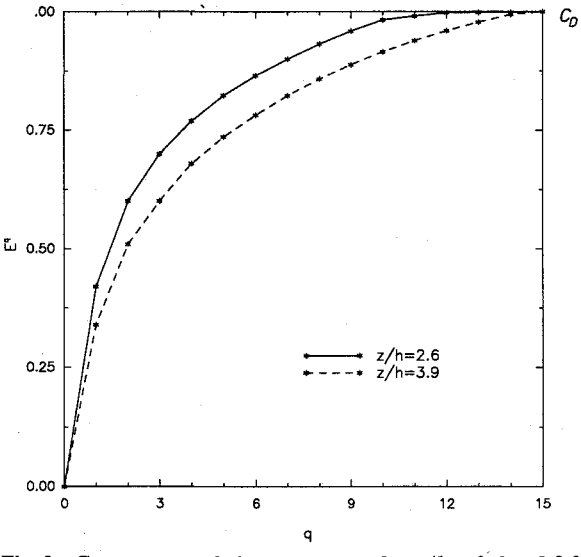

Fig. 2 Convergence of eigenspectra modes $z/h = 2.6$ and 3.9.

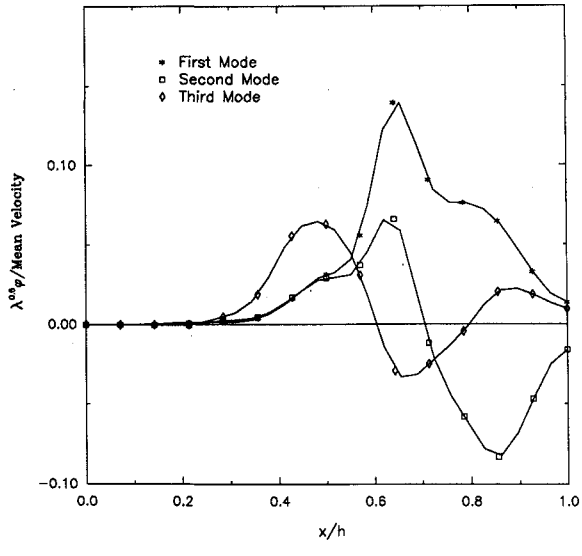

Fig. 3 First three eigenfunctions at $z/h = 2.6$.

Table 1 Percent energy in eigenspectral modes

Position Y/h, Z/h	First mode	First two modes	First three modes	First four modes	First five modes
0.75, 2.6	42	60	70	77	82
0.75, 3.9	34	51	60	68	74
0.50, 2.6	41	56	67	75	81
0.50, 3.9	24	40	53	63	70
0.25, 3.9	32	50	61	68	75
0.00, 2.6	27	45	56	67	73

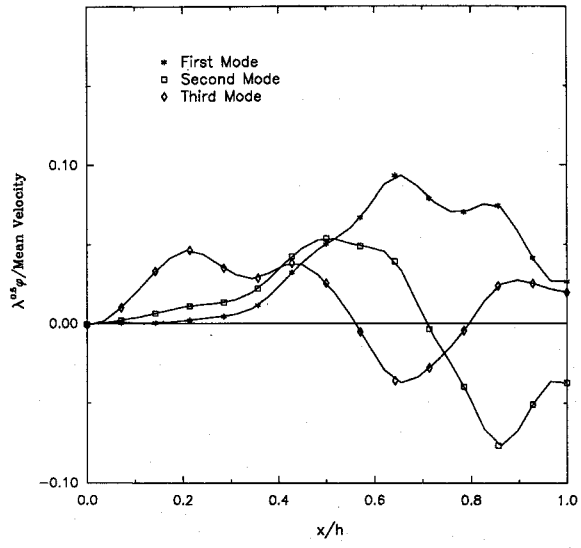

Fig. 4 First three eigenfunctions at $z/h = 3.9$.

Eigenfunctions

To avoid having to choose a particular frequency at which to examine the cross-stream behavior of the eigenfunctions, it is convenient to suppress the frequency behavior. This results in a one-dimensional version of the POD where only the x direction is studied. This is achieved by integrating $\Phi_{11}(x, x', \bar{y}, \bar{z}, f)$ over frequency to obtain $R_{11}(x, x', \bar{y}, \bar{z})$, which then

becomes the kernel in the integral eigenvalue problem that is written as

$$\int R_{11}(x, x', \bar{y}, \bar{z})\psi_1^{(n)}(x', \bar{y}, \bar{z})\, dx' = \lambda^{(n)}\psi_1^{(n)}(x, \bar{y}, \bar{z}) \quad (6)$$

This equation is then solved for each downstream location and the x dependency of the eigenfunctions examined and compared for both locations.

Figures 3 and 4 show the eigenfunctions, weighted by $\lambda^{0.5}$ and normalized by the mean velocity, for both $z/h = 2.6$ and 3.9, respectively. These eigenfunctions behave the same as other typical orthogonal eigenfunctions, i.e., the higher the mode the more zero crossings. This is consistent with the findings of Moin and Moser[12] in turbulent channel flow and Glauser et al.[14] in the axisymmetric jet. Note how the first mode is more spatially compact at $z/h = 2.6$ than at $z/h = 3.9$. The higher POD modes exhibit this behavior as well. These results indicate that the flow has evolved to a more homogeneous state by $z/h = 3.9$.

The contribution of the qth POD mode to the rms velocities u' can be obtained from the eigenvalues and eigenfunctions as

$$[u'(x)]^q = \sum_{n=1}^{q} [\lambda^{(n)}\psi_1^{(n)}(x)\psi_1^{(n)*}(x)]^{0.5} \quad (7)$$

Figures 5 and 6 show the rms streamwise fluctuating velocity, plotted vs x position, for the two downstream positions with their reconstruction using Eq. (7) for $q = 1$, 3, and 5 superimposed. For both downstream locations, the first POD mode ($q = 1$) contains the highest percentage of streamwise turbulent kinetic energy at the spatial location with the most energy (wire 10, $x/h = 0.71$). Also, for both downstream locations the first POD mode contributes significantly to the rms profiles with that at $z/h = 2.6$ being about 10% greater than that at $z/h = 3.9$. This implies that the structure has dissipated somewhat (spread out spatially) by $z/h = 3.9$, consistent with what was observed in the eigenfunction analysis and the results of the previous section. It can also be inferred from these figures that subsequent modes fill in the energy at the other spatial locations until the profile has been reproduced. Note that the first POD eigenfunctions, weighted by $\lambda^{0.5}$, are identical to the first POD mode reconstructions of the rms values. Also note how the dominant eigenfunctions at both streamwise locations exhibit similar behavior to the rms velocity profiles at their respective positions. This suggests that a rough idea of the spatial structure of the dominant eigenfunctions may be inferred (not the amplitude) from the single point rms velocity measurements.

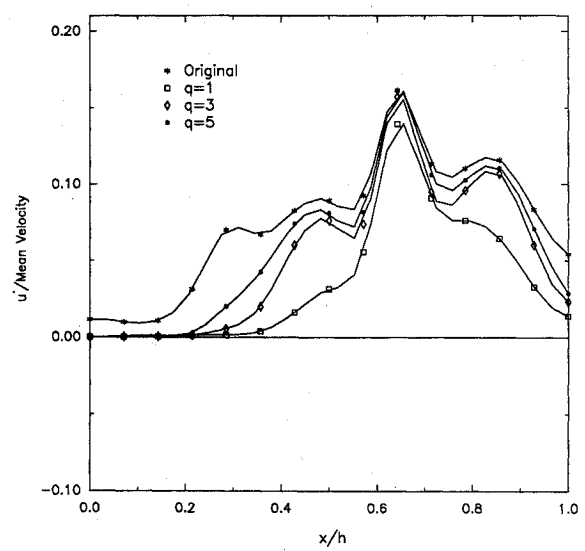

Fig. 5 Streamwise rms velocity (original and $q = 1$, 3, and 5) $z/h = 2.6$.

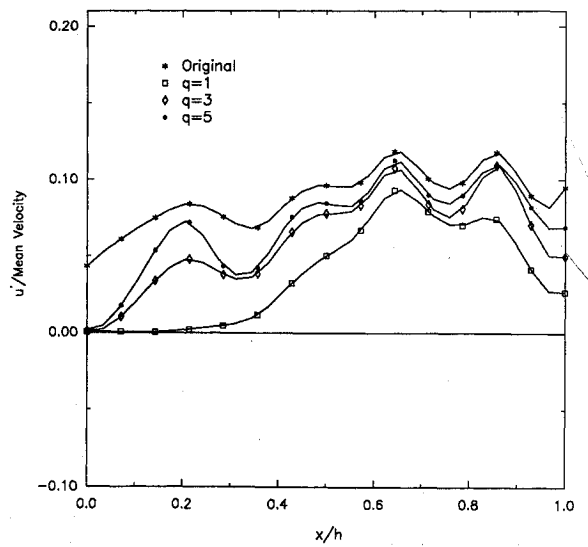

Fig. 6 Streamwise rms velocity (original and $q = 1$, 3, and 5) $z/h = 2.9$.

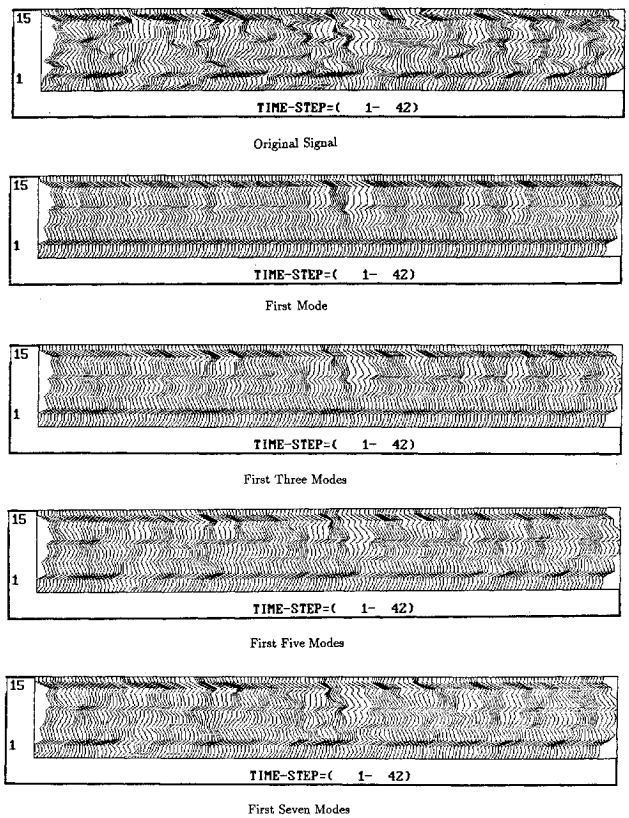

Fig. 7 Pseudoflow visualization plots $z/h = 2.6$.

Instantaneous Velocity

In this section the instantaneous velocities and the contribution to them from the various POD eigenmodes are examined at both downstream locations by using a pseudoflow visualization technique. A variation of Eq. (3), similar in concept to what was done in the previous two sections, can be derived, for the contribution of the qth POD mode to the instantaneous velocity, as

$$[u_1(x, t)]^q = \int_{-\infty}^{\infty} \sum_{n=1}^{q} a_n(f)\psi_1^{(n)}(x, f)e^{i2\pi ft}\, df \quad (8)$$

In this case, when q goes to N, the original velocity will be obtained. The pseudoflow visualization technique used here is similar to that developed by Tabatabai et al.[22] and Delville et al.[7] and is described in more detail by Ukeiley et al.[6] Briefly, the simultaneous hot-wire anemometer data are used to create

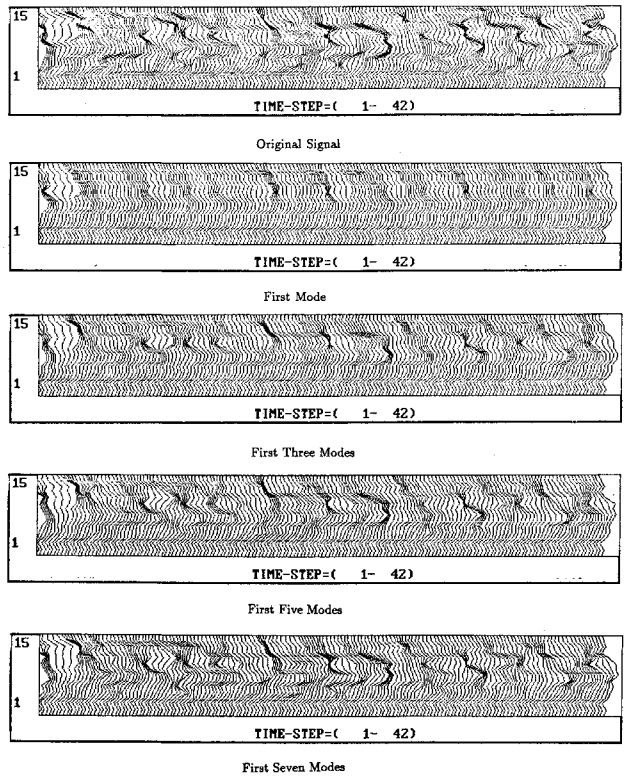

Fig. 8 Pseudoflow visualization plots $z/h = 3.9$.

a graphical representation of velocity interactions in a flowfield. Since the velocities are sampled simultaneously, *instantaneous* velocity profiles can be obtained, which are then plotted for each time step.

Figures 7 and 8 show pseudoflow visualization plots for $z/h = 2.6$ and 3.9, respectively. These plots have wire number as the abscissa and time sample number as the ordinate. The figures compare the original signal with reconstructions using $q = 1$, 3, 5, and 7 in Eq. (8). The idea of viewing the reconstruction of the velocity field from application of the POD through a pseudoflow visualization technique was first implemented by Delville et al.[17] From examination of Figs. 7 and 8 it is evident that the first mode representations have the large-scale (global) features of the original streamwise velocity field. This is consistent with the speculation that low dimensional models for turbulence, based on the first POD mode, are capturing the overall picture (Aubry et al.,[23] Glauser et al.,[24] and Deane et al.[25]). It is also apparent that the structures are not quite as evident at $z/h = 3.9$ as those at $z/h = 2.6$ and that, as more modes are used in the reconstruction process, additional small-scale features are represented. The pseudoflow visualization plots using the summation of the first seven modes are similar to the original signals at both downstream positions. However, the seven-mode reconstruction is more representative of the original signal at $z/h = 2.6$ than at $z/h = 3.9$, consistent with the results presented in Table 1 and Fig. 2.

Conclusions

An investigation studying the streamwise evolution of large-scale structures in the downstream region of the lobed mixer was conducted through the implementation of a two-dimensional scalar version of the POD. The dominant eigenmodes contain a greater portion of the relative streamwise kinetic energy closer to the trailing edge of the mixer ($z/h = 2.6$ compared with $z/h = 3.9$) for all vertical (y/h) positions. For both downstream locations the POD eigenfunctions behave the same as other typical orthogonal functions; that is, the higher the mode, the more zero crossing. The spatial behavior of the first POD modes tend to exhibit similar characteristics to the rms streamwise velocity profiles and evolve, in the downstream direction, in much the same manner. The pseudoflow visualizations of the first POD mode representations of the instantaneous velocity fields exhibit the large-scale (global) features of the original fields, with the structures more evident closer to the trailing edge of the mixer. The pseudoflow visualizations of the contributions from the first seven modes are similar to the original signals at both downstream positions, with the seven-mode reconstruction more representative of the original signal at the position closer to the trailing edge of the mixer. All of these results indicate that the large-scale structures are breaking down and the flow is becoming more homogeneous between the two downstream locations examined in this study.

Acknowledgments

This research was initiated under support from Pratt and Whitney/UTC. Work was continued under support from the Cornell Clarkson NASA Space Grant Consortia and NSF Grant INT-9016045.

References

[1]Ukeiley, L., Varghese, M., Glauser, M., and Valentine, D., "Multifractal Analysis of a Lobed Mixer Flowfield Utilizing the Proper Orthogonal Decomposition," *AIAA Journal,* Vol. 30, No. 5, 1992, pp. 1260–1267.

[2]Werle, M. J., Presz, W., and Paterson, R. W., "Flow Structure in a Periodic Axial Vortex Array," AIAA Paper 87-0160, Jan. 1987.

[3]Paterson, R. W., "Turbofan Mixer Nozzle Flowfield—A Benchmark Experimental Study," *ASME Journal of Engineering for Gas Turbines and Power,* Vol. 106, 1982, pp. 692–698.

[4]Eckerle, W. A., Sheibani, H., and Awad, J., "Experimental Measurements of the Vortex Development Downstream of a Lobed Forced Mixer," American Society of Mechanical Engineers, ASME 90-GT-27, June 1990.

[5]Koutmos, P., and McGuirk, J. J., "Isothermal Velocity and Turbulence Measurements Downstream of a Model Multilobed Turbofan Mixer," *Experiments in Fluids,* Vol. 8, 1989, pp. 183–191.

[6]Ukeiley, L., Wick, D., and Glauser, M., "Coherent Structure Identification in a Lobed Mixer," American Society of Mechanical Engineers, ASME 91-GT-307, Orlando, FL, June 1991.

[7]Delville, J., Bellin, S., Garem, J. H., and Bonnet, J. P., "Analysis of Structures in a Turbulent Plane Mixing Layer by Use of a Pseudo Flow Visualization Method Based Hot-Wire Anemometry," *Advances in Turbulence II,* edited by H. H. Fernholtz and H. E. Fielder, Springer-Verlag, Berlin, 1988, pp. 251–256.

[8]Kock am Brink, B., and Foss, J., "Streamwise Vorticity Measurements in the Wake of a Rippled and Planar Trailing Edge," Michigan State Univ. Rept. MSU-ENG-91-009, East Lansing, MI, 1991.

[9]Lasheras, J. C., and Choi, H., "Three-Dimensional Instability of a Plane Free Shear Layer: An Experimental Study of the Formation and Evolution of Streamwise Vortices," *Journal of Fluid Mechanics,* Vol. 189, 1988, pp. 53–86.

[10]Lumley, J. L., "The Structure of Inhomogeneous Turbulent Flows," *Atmospheric Turbulence and Radio Wave Propagation,* edited by A. M. Yaglom and V. I. Tatarsky, Nauka, Moscow, Russia, 1967, pp. 166–178.

[11]Lumley, J. L., *Stochastic Tools in Turbulence,* Academic Press, New York, 1970.

[12]Moin, P., and Moser, R. D., "Characteristic-Eddy Decomposition of Turbulence in a Channel," *Journal of Fluid Mechanics,* Vol. 200, 1989, pp. 471–509.

[13]Herzog, S., "The Large Scale Structure in the Near-Wall of Turbulent Pipe Flow," Ph.D. Dissertation, Sibley School of Mechanical and Aerospace Engineering, Cornell Univ., Ithaca, NY, 1986.

[14]Glauser, M. N., Zheng, X., and George, W. K., "An Analysis of the Turbulent Axisymmetric Jet Mixing Layer Utilizing the Proper Orthogonal Decomposition," *Journal of Fluid Mechanics* (accepted for publication, 1993).

[15]Sirovich, L., Maxey, M., and Tarman, H., "Analysis of Turbulent Thermal Convection," *Proceedings of the Sixth Symposium on Turbulent Shear Flows* (Toulouse, France), 1987, pp. 12.5.1-12.5.6.

[16]Chambers, D. H., Adrian, R. J., Moin, P., Stewart, D. S., and Sung, H. J., "Karhunen-Loeve Expansion of Burgers' Model of Turbulence," *Physics of Fluids,* Vol. 31, No. 9, 1988, pp. 2573–2582.

[17]Delville, J., Bellin, S., and Bonnet, J. P., "Use of the Proper Orthogonal Decomposition in a Plane Turbulent Mixing Layer," *Turbulence and Coherent Structures,* edited by O. Metais and M.

Lesieur, Kluwer Academic Publishers, Dordrecht, The Netherlands, pp. 75–90.

[18]Loeve, M., *Probability Theory,* Van Nostrand, Princeton, NJ, 1955.

[19]Glauser, M. N., Leib, S. J., and George, W. K., "Coherent Structures in the Axisymmetric Jet Mixing Layer," *Turbulent Shear Flows 5,* edited by F. Durst et al., Springer-Verlag, Berlin, 1987, pp. 134–145.

[20]Ukeiley, L., Wick, D., and Glauser, M., "A Novel Hot-Wire Rake Design," American Society of Mechanical Engineers, ASME FED-Vol 97, June 1990, pp. 87–92.

[21]George, W. K., Beuther, P. D., and Shabbir, A., "Polynomial Calibrations for Hot Wires in Thermally-Varying Flow," American Society of Mechanical Engineers, ASME FED-Vol. 53, June 1987, pp. 3–6.

[22]Tabatabai, M., Kawall, J. G., and Keffer, J. F., "Flow Visualization Using Hot-Wire Anemometry," *Dantec Information,* Vol. 04, 1987.

[23]Aubry, N., Holmes, P., Lumley, J. L., and Stone, E., "The Dynamics of Coherent Structures in the Wall Region of a Turbulent Boundary Layer," *Journal of Fluid Mechanics,* Vol. 192, 1988, pp. 115–173.

[24]Glauser, M. N., Zheng, X., and Doering C. R., "The Dynamics of Organized Structures in the Axisymmetric Jet Mixing Layer," *Turbulence and Coherent Structures,* edited by O. Metais and M. Lesieur, Kluwer Academic Publishers, Dordrecht, The Netherlands, 1991, pp. 253–265; also see *Physics of Fluids A* (submitted for publication).

[25]Deane, A. E., Kevrekidis, I. G., Karniadakis, G. E., and Orszag, S. A., "Low Dimensional Models for Complex Geometry Flow: Application to Grooved Channels and Circular Cylinders," *Physics of Fluids A,* Vol. 3, No. 10, 1991, pp. 2337–2354.